

# Scalable Probabilistic Matrix Factorization with Graph-Based Priors

Jonathan Strahl<sup>1</sup>, Jaakko Peltonen<sup>2</sup>, Hiroshi Mamitsuka<sup>1,3</sup>, and Samuel Kaski<sup>1</sup>

<sup>1</sup>Helsinki Institute for Information Technology HIIT,  
Department of Computer Science, Aalto University

<sup>2</sup>Faculty of Information Technology and Communication Sciences,  
Tampere University, Finland

<sup>3</sup>Bioinformatics Center, Institute for Chemical Research, Kyoto  
University, Japan

February 15, 2022

## Abstract

In matrix factorization, available graph side-information may not be well suited for the matrix completion problem, having edges that disagree with the latent-feature relations learnt from the incomplete data matrix. We show that removing these *contested* edges improves prediction accuracy and scalability. We identify the contested edges through a highly-efficient graphical lasso approximation. The identification and removal of contested edges adds no computational complexity to state-of-the-art non-probabilistic graph-regularized matrix factorization, remaining linear with respect to the number of non-zeros. Computational load even decreases proportional to the number of edges removed. Formulating a probabilistic generative model and using expectation maximization guarantees convergence. Rich simulated experiments illustrate the desired properties of the resulting algorithm. On real data experiments we demonstrate improved prediction accuracy on four out of five experiments (empirical evidence that graph side-information is often inaccurate), and the same prediction accuracy with 20% fewer edges. A 300 thousand dimensional graph with 3 million edges can be analyzed in under ten minutes on a standard laptop computer.

## 1 Introduction

Matrix factorization (MF) is popular in a number of domains including recommender systems [28, 36], bioinformatics [6, 26, 47, 52, 56], image restoration

[50] and many more [12]. Much of the data is of a very large scale and sparse, and additional (side-)information is usually available. Therefore, many methods focus on scalability [12, 37, 42] and the addition of side information (SI) [11, 10, 20, 33, 52, 57, 55], and more recently scalable methods with SI [38, 40, 51].

Empirical evidence shows that prediction accuracy is significantly improved by graph SI, where edges in the graph represent similarity between connected nodes [7, 33, 38, 40, 51, 57, 55]. MF (or low-rank matrix completion) has theoretical guarantees for exact completion without and with noise [8, 9]. Introducing noisy SI is shown to reduce sample-complexity, and is reduced even further handling the noise [11]. Reduction in sample complexity through the introduction of graph SI has also been shown [2, 40], as a function of graph quality. However, to the best of our knowledge there is no work on scalable methods to handle the noise in the graph SI.

Mnih and Salakhutdinov [37] introduced probabilistic matrix factorisation (PMF), which is equivalent to  $\ell_2$ -regularised (alternating least squares) MF. Probabilistic interpretations for MF with graph SI are kernelized PMF (KPMF [57]) and kernelized Bayesian MF (KBMF [20]): placing priors over the columns of the latent feature matrices. This type of prior models the pairwise relation between rows, where these rows correspond to rows or columns of the incomplete data matrix. KPMF and KBMF showed good results on moderate-sized data but failed to scale to large data.

To address scalability, graph-regularised least squares (GRALS [40]) was proposed, with conjugate gradient descent exploiting the sparsity in the data matrix and the graphs, resulting in linear computational complexity and fast convergence. Recently there has been progress on applying deep learning to this problem showing potential for scalability [4, 24, 38, 51], but with a slow convergence rate in practice (see supplementary material for empirical evidence).

All of the non-Bayesian or scalable methods incorporating graph SI [7, 33, 38, 40, 57] fix the edges in the graph, considering them as true. However, these graphs are known to be uncertain [1, 3], and furthermore, the similarities they represent (e.g. homophily [35]) are rarely specific to the matrix factorization task leaving no guarantee that correlations correspond [33, 44]; graphs are often formed for other purposes, and hence their usefulness for MF is uncertain. This leaves room for improving the quality of the graph, leading to a significant reduction in sample complexity [2]. In this work we will introduce a solution based on contested edges, defined later in the paper.

**Example of Graph Side-Information and Contested Edges** To better understand how graph similarities are not task-specific (are non-specific) to MF, take a common example of a movie-recommendation problem with social network (SN) SI ([33] and in our experiments on Douban data). Connected users in the SN do not connect based on their similar preference of movies, instead they connect on the basis of a broader social context. Similarly, the demographic information in MovieLens<sup>1</sup>, used to form a user-similarity graph, is

<sup>1</sup><https://grouplens.org/datasets/movielens/>

only very indirectly related to the movie preferences [35]. Nevertheless, more general similarity has been shown to often work well in practice, but some parts of it may turn out to be detrimental as we illustrate below.

Figure 1 (left) shows a small movie-recommendation data matrix with SN SI (middle). Without SI, if row/column observations in the data matrix are similar, latent features will be similar. This can be inaccurate, e.g. users 2 and 3 would be considered similar based on the observations, and thus predictions for user 2 would be similar to ratings of user 3, whereas actually user 2 is similar to user 1. Graph information can help by encouraging latent features of connected users, like user 1 and user 2 here, to be similar, even when there is no observed data in the matrix to indicate they should be. However, for other users such as 4 and 5 the graph may mismatch with the data, indicating similarity whereas 4 and 5 are actually negatively correlated (as seen in their ratings of movies 5 and 6), and using the graph would thus worsen their predictions. We propose using this discrepancy to *contest* the graph edge between users 4 and 5; removing this edge as in Figure 1 (right) would improve predictions for users 4 and 5 to be consistent with their observed negative correlation, while the beneficial edge between users 1 and 2 will still remain. In real cases, mismatch between the data matrix and the SI would be detected based on much more data than in this illustration.

We do not propose to identify contested edges directly from the observed data but from correlations between the latent features. We introduce a probabilistic generative model that we call graph-based prior PMF (GPMF). Using the expectation-maximization (EM, [5]) algorithm we find a maximum a posteriori (MAP) estimate for the latent features and a maximum likelihood estimate (MLE) for the correlations of the latent features. We show in Section 3.3 how using GLASSO approximation we can remove contested edges by simply thresholding a constrained sample covariance matrix (SCM).

There exist a number of approaches to reduce the edges in a labelled graph, graph summarization [32] for example. Most of these approaches do not use node attributes (labels) and to the best of our knowledge none use latent features for edge pruning. There are link prediction models that are probabilistic and use node attributes [22] but none of them can (yet) scale to large data [30, 39, 54].

This paper introduces GPMF: the generative model in Section 2, the scalable constrained EM algorithm in Section 3, experiments in Appendix B and a conclusion in Section 5.

## 2 GPMF Generative Model and Relations to the Graph Side-Information

We are provided with a partially observed data matrix  $\mathbf{R}$  with  $N$  rows and  $M$  columns.  $\mathbf{R}$  is approximated as the product of two low-rank matrices,  $\mathbf{U}$  and  $\mathbf{V}$ . The number of latent features  $D$  is fixed;  $\mathbf{U}$  and  $\mathbf{V}$  have  $D$  columns, each row is a latent feature vector for each row / column of  $\mathbf{R}$  respectively. We use

User	Movie						
	$m_1$	$m_2$	$m_3$	$m_4$	$m_5$	$m_6$	$m_7$
$u_1$	5		1				
$u_2$	5	4	1				
$u_3$	1	4	5				
$u_4$				5	4	2	1
$u_5$				1	2	4	5

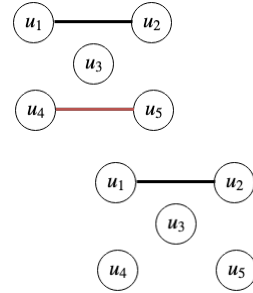


Figure 1: An illustrative movie recommendation problem. *Left:* data matrix where entries are user-ratings for movies: observations in black, unseen entries are blank and unseen entries to be predicted are in grey. *Middle:* Social Network SI; connected users assumed to have similar ratings. The edge shown in red is contested due to negative correlation of  $u_4$  and  $u_5$  in the data matrix. *Right:* a graph update with removal of the contested edge to improve prediction accuracy.

an index set  $\Omega$  where  $\Omega_{ij}$  is one if the element in row  $i$  and column  $j$  of  $\mathbf{R}$  is observed, and zero otherwise. The goal is to learn latent-feature matrices  $\mathbf{U}$  and  $\mathbf{V}$  that most accurately represent the full matrix  $\mathbf{R}$ .

$\ell_2$ -regularized MF has a scalable probabilistic interpretation: PMF. Each observed entry  $\mathbf{R}_{ij} : (i, j) \in \{\Omega = 1\}$  is assumed to have Gaussian noise  $\sigma^2$ ; each row of  $\mathbf{U}$  and  $\mathbf{V}$  has a zero-mean spherical Gaussian prior. Similar to KPMF [57], our model replaces the spherical Gaussian prior with a full-covariance Gaussian over the columns of the latent features (introducing row-wise dependencies):

$$p(\mathbf{R} | \mathbf{U}, \mathbf{V}, \sigma^2) = \prod_{i=1}^N \prod_{j=1}^M \mathcal{N}(\mathbf{R}_{ij} | \mathbf{U}_i \cdot \mathbf{V}_j^\top, \sigma^2)^{\Omega_{ij}} \quad (1)$$

$$p(\mathbf{U} | \Lambda_U) = \prod_{d=1}^D \mathcal{N}(\mathbf{U}_{:d} | \mathbf{0}, \Lambda_U^{-1}) \quad (2)$$

$$p(\mathbf{V} | \Lambda_V) = \prod_{d=1}^D \mathcal{N}(\mathbf{V}_{:d} | \mathbf{0}, \Lambda_V^{-1}). \quad (3)$$

Graph SI constrains the structure of the precision matrices ( $\Lambda_U$  or  $\Lambda_V$ ) of (2) and (3), discussed next.

## 2.1 Gaussian Markov Random Field (GMRF) relation to Precision matrix

An undirected graph  $\mathcal{G}_Z = (\mathcal{V}_Z, \mathcal{E}_Z)$  with a set of nodes  $\mathcal{V}_Z$ , representing a set of random variables  $\{Z_i\}_{i=1}^P$ , and a set of edges  $\mathcal{E}_Z \subseteq \{(i, j) | i, j \in \mathcal{V}_Z\}$ , defines the conditional independence of the random variables, where the absence of an edge  $(i, j) \notin \mathcal{E}_Z$  implies that the two random variables are conditionally

independent  $[\mathbf{A}_Z]_{ij} = 0$  given the remaining random variables [5, 25, 29, 41]:  $Z_i \perp Z_j \mid \{Z_k : k \in (1, \dots, N) \setminus (i, j)\}$ . In the remainder of the paper we refer to the adjacency matrix of  $\mathcal{G}_Z$ : a symmetric matrix where  $[\mathbf{A}_Z]_{ij}$  is one if an edge exists between nodes  $i$  and  $j$  and zero otherwise. We can summarize the GMRF relation as  $[\mathbf{A}_Z]_{ij} = 0 \iff [\mathbf{A}_Z]_{ij} = 0 \mid i \neq j$ .

## 2.2 Laplacian Matrix relation to Precision Matrix

The Laplacian matrix of a graph is  $\mathbf{L}_Z = \mathbf{D} - \mathbf{A}_Z$ , where  $\mathbf{D}_{i,i} = \sum_{j=1}^N [\mathbf{A}_Z]_{ij}$  is a diagonal degree matrix, and is positive-semi-definite by definition. The regularised Laplacian  $\mathbf{L}_Z^+ = \mathbf{L}_Z + \gamma \mathbf{I}$ ,  $\gamma > 0$  is a positive-definite matrix; a valid precision matrix retaining the GMRF property [14, 16, 17, 25, 31]:  $[\mathbf{L}_Z^+]_{ij} = 0 \iff [\mathbf{A}_Z]_{ij} = 0 \mid i \neq j$ .

**Lemma 1.** *If the precision matrix in (2) and (3) is the regularised Laplacian matrix  $\mathbf{L}_U^+, \mathbf{L}_V^+$ , then the MAP estimator of our model has the same objective function as GRALS [40]. Our GPMF model therefore gives a generalization of the GRALS objective function.*

*Proof of Lemma 1.* Our generative model is biconvex, and hence it suffices to prove for  $\mathbf{U}$  that the posterior is equivalent to the GRALS objective. Holding  $\mathbf{V}$  fixed and finding the log posterior of  $\mathbf{U}$ :

$$\begin{aligned} \ln p(\mathbf{U} | \mathbf{R}, \sigma^2, \mathbf{V}, \mathbf{A}_U) &\propto \ln p(\mathbf{R} | \mathbf{U}, \mathbf{V}, \sigma^2) p(\mathbf{U} | \mathbf{A}_U) \\ &\propto -\frac{1}{\sigma^2} \sum_{i=1}^N \sum_{j=1}^M \mathcal{P}_\Omega(\mathbf{R}_{ij} - \mathbf{U}_i \mathbf{V}_j)^2 - \frac{1}{2} \sum_{d=1}^D \mathbf{U}_{:d}^\top \mathbf{A}_U \mathbf{U}_{:d} \\ &= -\frac{1}{2} \|\mathcal{P}_\Omega(\mathbf{R} - \mathbf{U}\mathbf{V}^\top)\|_{\mathbb{F}}^2 - \frac{\sigma^2}{2} \text{tr}(\mathbf{U}^\top \mathbf{L}_U^+ \mathbf{U}), \end{aligned} \quad (4)$$

where  $\mathbf{U}_i$  is row  $i$  of matrix  $\mathbf{U}$  and  $\mathbf{U}_{:d}$  is column  $d$  and noting that  $\sum_{i,j} \mathbf{U}_{ij}^2 = \text{tr}(\mathbf{U}^\top \mathbf{U}) = \|\mathbf{U}\|_{\mathbb{F}}^2$ . Equation (4) is the GRALS objective function [40]. Derivations in the supplementary material.  $\square$

## 3 GRAEM: Scalable EM for GPMF

We naturally extend each least-squares sub-problem of GRALS [40] with graph-regularised alternating EM (GRAEM), having the same global convergence guarantees as GRALS [49]. We work through optimising  $\mathbf{U}$  with  $\mathbf{V}$  fixed, solving for  $\mathbf{V}$  has the same form.

### 3.1 The EM Formulation

We have an incomplete data matrix  $\mathbf{R}$ , fixed matrix  $\mathbf{V}$ , latent variable matrix  $\mathbf{U}$ , and graph SI. From the graph we derive  $\mathbf{L}_U^+$  (see Section 2.2), then set the precision matrix  $\mathbf{A}_U = \mathbf{L}_U^+$ , which we consider our model parameters. We want

to maximize the expectation of the joint density of the data and the latent variables, with  $\mathbf{U}$  as our unknowns and  $\mathbf{\Lambda}_U$  as our input parameters:

$$\mathcal{Q}(\mathbf{\Lambda}_U, \mathbf{\Lambda}_U^{\text{old}}) = \int_{\mathbf{U}} p(\mathbf{U}|\mathbf{R}, \mathbf{\Lambda}_U^{\text{old}}) \ln p(\mathbf{R}, \mathbf{U} | \mathbf{\Lambda}_U) d\mathbf{U} = \mathbb{E}_{p(\mathbf{U}|\mathbf{R}, \mathbf{\Lambda}_U^{\text{old}})} [\ln p(\mathbf{R}, \mathbf{U} | \mathbf{\Lambda}_U)] . \quad (5)$$

### 3.2 E-step: Expected Value of the Latent Variables

The expected value of our latent variables has a Gaussian posterior distribution (see supplementary material), we can therefore use the MAP, which is equivalent to the GRALS objective function as shown in lemma 1:  $\mathbb{E}_{p(\mathbf{U}|\mathbf{R}, \mathbf{\Lambda}_U^{\text{old}})}[\mathbf{U}] = \boldsymbol{\mu}_U^{\text{post.}} \approx \hat{\boldsymbol{\mu}}_U^{\text{MAP}}$ .

### 3.3 M-step: Removing Contested Edges

We can remove edges in the graph that correspond to negative correlations between the latent features by simply removing negative covariances from an SCM; this relationship holds for large scale and sparse problems; details follow.

#### 3.3.1 The MLE of the parameters and GLASSO

To find the MLE we maximise the  $\mathcal{Q}$  function in Equation (5) with respect to  $\mathbf{\Lambda}_U$ . The maximum can be found in closed form by taking the derivative with respect to the parameter  $\mathbf{\Lambda}_U$  and setting to zero:

$$\arg \max_{\mathbf{\Lambda}_U} \mathcal{Q}(\mathbf{\Lambda}_U, \mathbf{\Lambda}_U^{\text{old}}) = \left( \mathbb{E}_{p(\mathbf{U}|\mathbf{R}, \mathbf{\Lambda}_U^{\text{old}})} \left[ \frac{1}{D} \sum_{d=1}^D \mathbf{U}_{:d} \mathbf{U}_{:d}^\top \right] \right)^{-1} = \left( \mathbb{E} [\mathbf{S}_U^D] \right)^{-1} = \mathbf{\Lambda}_U^* . \quad (6)$$

Equation (6) is the inverse of an SCM, where each sample is one of the columns of  $\mathbf{U}$ . Values for  $\mathbf{U}$  are unknown, so we use the MAP given the previous estimate of the parameters ( $\mathbf{\Lambda}_U^{\text{old}}$ ). The solution (if any) is almost surely not sparse. Graphical lasso (GLASSO [34]) finds a sparse solution for the MLE of the precision matrix, where samples are assumed to be normally distributed, in line with our model assumptions in Section 2. We therefore propose solving (6) with GLASSO.

#### 3.3.2 Constrained GLASSO and Highly Efficient Approximation

GLASSO finds the MLE of the precision matrix under an  $\ell_1$  penalty, given an SCM  $\mathbf{S}$ . [21] showed that the problem space can be reduced with prior knowledge on which pairwise relationships do not exist, forcing them to be zero in the solution:

$$\min_{\mathbf{\Lambda}_U \succeq 0} \text{tr}(\mathbf{S}\mathbf{\Lambda}_U) - \log |\mathbf{\Lambda}_U| + \tau \|\mathbf{\Lambda}_U\|_1, \quad \text{subject to } [\mathbf{\Lambda}_U]_{ij} = 0, [\mathbf{A}_U^0]_{ij} = 0 . \quad (7)$$

[53] uses a relation between the sparsity structure of the  $\tau$ -thresholded SCM and the GLASSO solution; for large-scale problems, when the solution is very sparse, the connected components are equivalent [34], given further assumptions the complete sparsity structure is equivalent [19, 45, 46]. However, this solution will locate correlations, positive and negative, with a strong magnitude, greater than  $\tau$ . Next we detail how to identify edges that correspond to only negative correlations.

### 3.3.3 Removing a Contested Edge

The sparsity structure of the SCM and the (GLASSO) solution are equivalent under mild assumptions that are found to be true for sufficiently large  $\tau$ , that result in  $\approx 10N$  non-zeros in the solution [18, 19]. One of these assumptions is sign-consistency where each non-zero element of the solution has the opposite sign in the SCM. Assuming sign-consistency we can identify all graph edges that correspond to negative correlations in the latent features, with  $\mathbb{E}[\mathbf{S}_U^D]$  from Equation (6) as our SCM:

$$[\mathbf{A}_U^{\text{new}}]_{ij} = \begin{cases} 1, & [\mathbf{A}_U^0]_{ij} = 1, \mathbb{E}[\mathbf{S}_U^D]_{ij} \geq \tau \\ 0, & [\mathbf{A}_U^0]_{ij} = 1, \mathbb{E}[\mathbf{S}_U^D]_{ij} < \tau, \text{ contested edge identified} \\ 0, & \text{otherwise,} \end{cases} \quad \text{constrained edge,} \quad (8)$$

where  $\mathbf{A}_U^{\text{new}}$  is the updated adjacency matrix, the threshold parameter  $\tau$  is set to zero (or can be increased for a sparser solution) and  $\mathbf{A}_U^0$  is the adjacency matrix of the graph SI. To solve Equation (8) we need to compute  $\mathbb{E}[\mathbf{S}_U^D]$ , we can decompose the problem:

$$\mathbb{E}[\mathbf{U}_{:d}\mathbf{U}_{:d}^\top] = \text{Cov}[\mathbf{U}_{:d}] + \mathbb{E}[\mathbf{U}_{:d}]\mathbb{E}[\mathbf{U}_{:d}^\top] = \boldsymbol{\Sigma}_{U:d}^{\text{post.}} + [\boldsymbol{\mu}_{U:d}^{\text{post.}}] [\boldsymbol{\mu}_{U:d}^{\text{post.}}]^\top,$$

where  $\mathbb{E}[\mathbf{S}_U^D] = \frac{1}{D} \sum_{d=1}^D \mathbb{E}[\mathbf{U}_{:d}\mathbf{U}_{:d}^\top]$ . The remaining task is to efficiently approximate the posterior covariance  $\boldsymbol{\Sigma}_{U:d}^{\text{post.}}$  for each column,  $d$ , of  $\mathbf{U}$ , which we discuss next.

### 3.3.4 Posterior Covariance Approximation

The posterior of our GPMF model, in Section 2, is a joint Gaussian distribution, where the likelihood in Equation (1) introduces relations between the columns of the latent features and the prior in Equation (2) introduces relations between the rows. This results in a posterior covariance matrix with an inverse Kronecker sum structure [27, 43]:  $\boldsymbol{\Sigma}_U^{\text{post.}} = (\mathbf{I}_D \otimes \boldsymbol{\Lambda}_U + \alpha \mathbf{C})^{-1}$  where  $\otimes$  is the Kronecker product operator and

$$\mathbf{C} = [\mathbf{c}(d, d')]_{d, d'=1}^D, \quad \mathbf{c}(d, d') = \text{diag} \left( \left\{ \sum_{j=1}^M \boldsymbol{\Omega}_{ij} \mathbf{V}_{jd} \mathbf{V}_{jd'} \right\}_{i=1}^N \right). \quad (9)$$

**Column-wise independence assumption.** We simplify the Kronecker sum with a column-wise independence assumption, setting all off-diagonals of  $\mathbf{C}$  to zero:

$$\boldsymbol{\Lambda}_U^{\text{post.}} \approx I_D \otimes \boldsymbol{\Lambda}_U + \alpha \text{diag}(\mathbf{C}) = \text{blkdiag} \left( \left\{ \hat{\boldsymbol{\Lambda}}_{U:d}^{\text{post.}} \right\}_{d=1}^D \right), \quad (10)$$

$$\hat{\boldsymbol{\Lambda}}_{U:d}^{\text{post.}} = \boldsymbol{\Lambda}_U + \alpha \text{diag}(\mathbf{C}_d), \quad \text{diag}(\mathbf{C}_d) = \text{diag} \left( \left\{ \sum_{j=1}^M \boldsymbol{\Omega}_{i,j} \mathbf{V}_{j,d}^2 \right\}_{i=1}^N \right),$$

where  $\alpha = [\sigma^2]^{-1}$  is the inverse of the observation noise in (1),  $\text{diag}$  takes a vector to create a diagonal matrix and  $\text{blkdiag}$  takes a sequence of matrices to construct a block-diagonal matrix.

**Sparse Cholesky factorisation:** Each  $\hat{\boldsymbol{\Lambda}}_{U:d}^{\text{post.}}$  is still too large to invert. Assuming the high-dimensional matrix is sparse, as in [53], its Cholesky factorisation is computable in  $\mathcal{O}(N)$  time [13]. We compute  $K$  samples as an unbiased estimate for the approximate posterior covariance:

$$\hat{\boldsymbol{\Sigma}}_{U:d}^{\text{post.}} = \left[ \hat{\boldsymbol{\Lambda}}_{U:d}^{\text{post.}} \right]^{-1} \approx \frac{1}{K} \sum_{k=1}^K \mathbf{x}_k \mathbf{x}_k^\top, \quad \mathbf{x}_k \sim \mathcal{N} \left( \mathbf{0}, \left[ \hat{\boldsymbol{\Lambda}}_{U:d}^{\text{post.}} \right]^{-1} \right).$$

### 3.4 The Algorithm

The EM algorithm iterates between E-step and M-step until convergence. We initialize the latent feature matrices ( $\mathbf{U}, \mathbf{V}$ ) by finding the MAP with no graph SI using PMF, to learn latent features that reflect the observed entries of the data matrix. In practise any method to learn the latent features with no SI can be used. The M step uses the relations between the latent features to identify negative correlations and remove them from the graph SI. The E-step then finds the MAP of the latent features given the updated graph. In theory the E and M step could be continued until some convergence criterion was met, but this would be less efficient and we get good results with just one step. So the three steps of our algorithm are lines 1,3 and 4:

### 3.5 Scalability: Computational Complexity

The algorithm has three steps: lines 1,3,4 in Algorithm 1. Line 1 is linear in the number of non-zeros  $nz()$  in the data matrix  $\mathcal{O}(nz(\boldsymbol{\Omega}))$  per conjugate gradient



---

**Algorithm 1** Graph-regularised alternating EM (GRAEM) algorithm

---

- Input:**  $\mathbf{A}_U^0, \mathbf{A}_V^0$   
**Output:**  $\hat{\mathbf{U}}, \hat{\mathbf{V}}$  and sparsified graphs  $\mathbf{A}_U^+, \mathbf{A}_V^+$
- 1:  $\mathbf{U}^0, \mathbf{V}^0 \leftarrow$  Initialise with PMF (GRALS with no graphs)
  - 2: **while** not converged **do**
  - 3:  $\mathbf{A}_U^t, \mathbf{A}_V^t \leftarrow$  Run M-step with  $\mathbf{U}^{t-1}, \mathbf{V}^{t-1}$  and  $\mathbf{A}_U^0, \mathbf{A}_V^0$  as structural constraints
  - 4:  $\mathbf{U}^t, \mathbf{V}^t \leftarrow$  Run E-step with regularized Laplacians given  $\mathbf{A}_U^t, \mathbf{A}_V^t$
  - 5: **end while**
- 

(CG) iteration. Line 3 comprises sparse Cholesky factorisation, linear in time with respect to the dimension size  $\mathcal{O}(N + M)$ , constrained SCM computation and thresholding,  $\mathcal{O}(nz(\mathbf{A}_U) + nz(\mathbf{A}_V))$  both converge in one time step. Line 4 uses GRALS with the sparsified graphs:  $\mathcal{O}(nz(\mathbf{\Omega}) + nz(\mathbf{A}_U^+) + nz(\mathbf{A}_V^+))$  per CG iteration. Line 4 is initialised with U,V values from the PMF run, largely reducing the number of iterations required. Our algorithm remains linear with respect to the number of non-zeros. The additional M-step is a trivial additional cost, and if  $\mathbf{A}_U^+, \mathbf{A}_V^+$  are much sparser, reducing iteration costs in Line 3, the overall computational load can be less than GRALS using the original graphs.

## 4 Experiments

We compare our algorithm to a baseline with no graph SI (PMF, [37]), the current most scalable method, GRALS [40], less scalable methods KPMF [57] and KBMF [20]. We do not compare to deep learning methods [4, 24, 38, 51] with high computational demand as we focus on efficient methods to demonstrate the efficiency of our graph update step. Note however that for initialisation any method to learn latent features can be used and for the E-step any method with graph SI.

### 4.1 Experiments on Synthetic Data

To analyze the behaviour of our algorithm we generate a data matrix with a known underlying graph. Therefore we can replace true edges in the graph with corrupted edges (CEs) that contest the true underlying structure, controlling the accuracy of the graph SI. We use a block-diagonal regularised-Laplacian precision matrix. We generate a  $400 \times 400$  data matrix by Equations (1)-(3), with proportion of corrupted edges 0.3, observation noise 0.01, 7% observed values, and 40 latent dimensions; we vary these settings in the experiments below. See supplementary material for further details.

**Graph Fidelity.** In Figure 2 we vary the number of CEs. A graph with no CEs has fidelity one ( $F=1$ ), with all CEs  $F=0$ . GPMPF consistently improves prediction accuracy over methods with graph SI for  $F > 0$ , and performance is

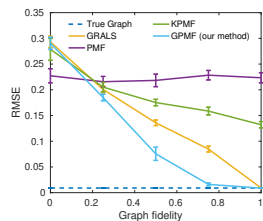


Figure 2: Decreasing contested edges

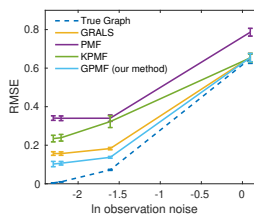


Figure 3: Increasing observation noise

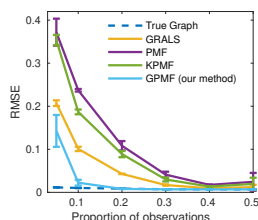


Figure 4: Increasing observed entries

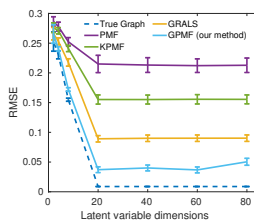


Figure 5: Increasing dimensionality

equal for  $F=0$ . PMF with no graph performs better below  $F=0.3$ , showing that a graph of low quality can make prediction accuracy worse.

**Observation Noise.** Figure 3 shows the benefit of GPMF diminishes as noise increases; learning negative correlations requires learning from the observations. However, at worst GPMF is only as bad as using the original corrupted graph.

**Proportion of Observations.** In Figure 4 with just 10% of observed entries our algorithm can almost attain the same prediction accuracy as using the true graph. GRALS requires 30% to achieve a similar accuracy. At 40% of observed entries the graph is no longer beneficial. Note that most large scale matrix completion problems have fewer than 10% observed entries.

**Model Capacity.** Figure 5 shows that with too few latent features all models are negatively effected, but overall GPMF attains the best prediction accuracy.

**GLASSO accuracy** We analyse the accuracy of removing CEs over several simulations. With 7% of observed entries 31.7% of CEs are removed and wrongly 19% of true edges (TEs), increasing to 40%, 44.3% of CEs are removed and 0.3% of TEs. Fixing observed entries at 20%, with noise  $\sigma^2 = 0.01$  39% CEs and 2.7% TEs are removed, and with  $\sigma^2 = 1$ , 34.3% CEs and 42.7% TEs are removed. We see clearly that observation noise strongly effects the ability to identify contested edges, reflected in Figure 3. Accuracy improves with more observed entries, but overall successful removal of CEs is only moderate (due to lack of observed entries and approximation inaccuracy). Regardless, experiments show this is enough to attain significant improvements in prediction accuracy.

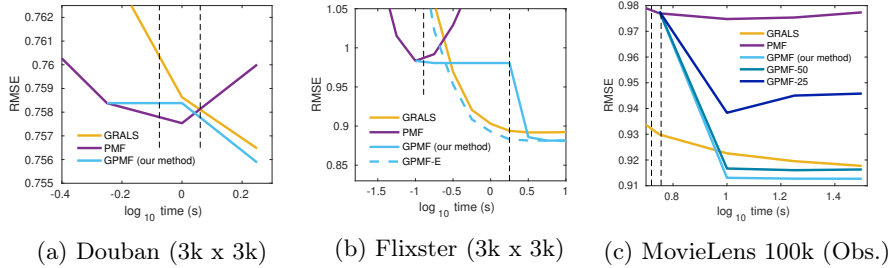


Figure 6: Convergence time; vertical lines show start and end of M-step, GPMF edge proportions a) 65% b) 55% c) 65%, GPMF-E is the E-step, GPMF-X uses a reduced graph with X prop. of edges.

## 4.2 Experiments on Real Data

In Figure 6 GPMF gives improved accuracy on all small datasets (3k by 3k subsets of Flixster and Douban [38], *full datasets not attainable*, and MovieLens100k [23]): in (c) we show that increasing the proportion of edges removed, decreases accuracy; improved convergence speed and accuracy using the updated graph for the E-step is shown in (b). In Figure 7 convergence speed is shown on large data (MovieLens20m [23], Epinions [48] and Yahoo Music [40, 15]), proportion of edges used by GPMF reported in figure title: (a) GPMF showed similar accuracy with fewer edges, this graph is extremely sparse and removing edges seems to give no gain; (b) graphs with  $k \in \{10, 20, 40\}$ -NN were tried and  $k = 40$  is plotted, results for all graphs in Table 1 show how GPMF improves with more neighbours (reducing sparsity) while the unaltered graphs reduce the accuracy of GRALS; (c) PMF outperformed GRALS indicating a poor-quality graph, our method improved prediction accuracy through removing contested edges. We also tested general usefulness of the updated graph: KPMF accuracy and convergence speed improved on Douban from 0.7322 to 0.7319 and we observed an increased convergence speed of a geometric deep learning model [38]. Note KBMF has many tuning parameters and we couldn't improve performance. Further details in supplementary material.

## 5 Conclusion

Formulating a probabilistic generative model with graph-based priors, GPMF, we introduce a highly scalable approach, GRAEM, to remove (contested) edges in graph SI that disagree with estimated latent-feature correlations. We show that thresholding the SCM of latent feature estimates can identify contested edges. The approach is linear in computational complexity, adding no cost to the current state-of-the-art scalable approach, GRALS. We also found the updated graph is beneficial for other models (even deep learning [38]) for this same task, suggesting the M-step in our algorithm to identify and remove contested edges

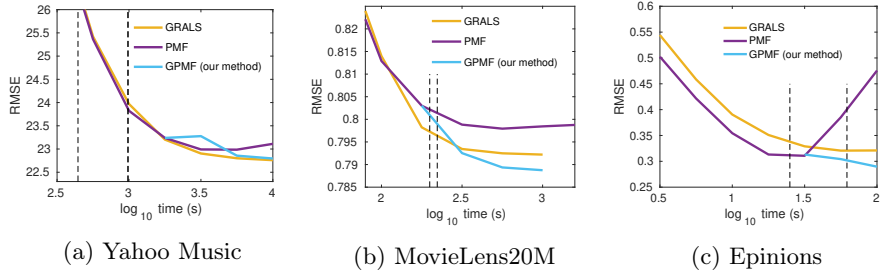


Figure 7: Convergence time; vertical lines show start and end of M-step. b) 40NN graph. GPMF proportion of edges used a) 80% b) 65% c) 45%

Table 1: Result summary on real datasets (RMSE)

ALGO.	FLIXSTER (3K)	DOUBAN (3K)	MOVIELENS 100K	EPINIONS	YAHOO MUSIC	MOVIELENS 20M (10-/20-/40-NN)
PMF	0.983	0.7575	0.194	0.31	22.991	0.7980 / 0.7980 / 0.7980
GRALS	0.892	0.7565	0.185	0.32	<b>22.760</b>	0.7898 / 0.7925 / 0.7922
GPMF (ours)	<b>0.881</b>	0.7559	<b>0.184</b>	<b>0.28</b>	22.795	<b>0.7894 / 0.7895 / 0.7887</b>
KPMF	0.921	<b>0.7322</b>	0.186	N/A	N/A	N/A
KBMF	0.977	0.8585	0.192	N/A	N/A	N/A
DATA DIMS.	3K x 3K	3K x 3K	1K x 1.5K	22K x 296K	250K x 300K	138K x 27K
NUM. OF OBS.	2.6K	137K	100K	824K	6M	20M

could be used in a wider domain.

## Acknowledgements

The research was partly funded by the Academy of Finland grant 313748 and Business Finland grant 211548, computational resources provided by the Aalto Science-IT project.

## References

- [1] Eytan Adar and Christopher Re. Managing uncertainty in social networks. *IEEE Data Eng. Bull.*, 30(2):15–22, 2007.
- [2] Kwangjun Ahn, Kangwook Lee, Hyunseung Cha, and Changho Suh. Binary rating estimation with graph side information. In *Advances in Neural Information Processing Systems*, pages 4272–4283, 2018.
- [3] Saurabh Asthana, Oliver D King, Francis D Gibbons, and Frederick P Roth. Predicting protein complex membership using probabilistic network reliability. *Genome research*, 14(6):1170–1175, 2004.
- [4] Rianne van den Berg, Thomas N Kipf, and Max Welling. Graph convolutional matrix completion. *arXiv preprint arXiv:1706.02263*, 2017.
- [5] Christopher M. Bishop. *Pattern Recognition and Machine Learning*. Springer, 2006.
- [6] Jean-Philippe Brunet, Pablo Tamayo, Todd R Golub, and Jill P Mesirov. Metagenes and molecular pattern discovery using matrix factorization. *Proceedings of the national academy of sciences*, 101(12):4164–4169, 2004.
- [7] Deng Cai, Xiaofei He, Jiawei Han, and Thomas S Huang. Graph regularized nonnegative matrix factorization for data representation. *IEEE Transactions on Pattern Analysis and Machine Intelligence*, 33(8):1548–1560, 2011.
- [8] Emmanuel J Candes and Yaniv Plan. Matrix completion with noise. *Proceedings of the IEEE*, 98(6):925–936, 2010.
- [9] Emmanuel J Candès and Benjamin Recht. Exact matrix completion via convex optimization. *Foundations of Computational mathematics*, 9(6):717, 2009.
- [10] Kai-Yang Chiang, Inderjit S. Dhillon, and Cho-Jui Hsieh. Using side information to reliably learn low-rank matrices from missing and corrupted observations. *Journal of Machine Learning Research*, 19(76):1–35, 2018.
- [11] Kai-Yang Chiang, Cho-Jui Hsieh, and Inderjit S Dhillon. Matrix completion with noisy side information. In C. Cortes, N. D. Lawrence, D. D. Lee, M. Sugiyama, and R. Garnett, editors, *Advances in Neural Information Processing Systems 28*, pages 3447–3455. Curran Associates, Inc., 2015.
- [12] Mark A Davenport and Justin Romberg. An overview of low-rank matrix recovery from incomplete observations. *IEEE Journal of Selected Topics in Signal Processing*, 10(4):608–622, 2016.
- [13] Timothy A Davis, John R Gilbert, Stefan I Larimore, and Esmond G Ng. A column approximate minimum degree ordering algorithm. *ACM Transactions on Mathematical Software (TOMS)*, 30(3):353–376, 2004.

- [14] Xiaowen Dong, Dorina Thanou, Pascal Frossard, and Pierre Vandergheynst. Learning laplacian matrix in smooth graph signal representations. *IEEE Transactions on Signal Processing*, 64(23):6160–6173, 2016.
- [15] Gideon Dror, Noam Koenigstein, Yehuda Koren, and Markus Weimer. The yahoo! music dataset and kdd-cup’11. In *Proceedings of the 2011 International Conference on KDD Cup 2011-Volume 18*, pages 3–18. JMLR.org, 2011.
- [16] Hilmi E Egilmez, Eduardo Pavez, and Antonio Ortega. Graph learning with laplacian constraints: Modeling attractive gaussian markov random fields. In *Signals, Systems and Computers, 2016 50th Asilomar Conference on*, pages 1470–1474. IEEE, 2016.
- [17] Hilmi E Egilmez, Eduardo Pavez, and Antonio Ortega. Graph learning from data under laplacian and structural constraints. *IEEE Journal of Selected Topics in Signal Processing*, 11(6):825–841, 2017.
- [18] Salar Fattahi and Somayeh Sojoudi. Graphical lasso and thresholding: Equivalence and closed-form solutions. *arXiv preprint arXiv:1708.09479*, 2017.
- [19] Salar Fattahi and Somayeh Sojoudi. Graphical lasso and thresholding: equivalence and closed-form solutions. *The Journal of Machine Learning Research*, 20(1):364–407, 2019.
- [20] Mehmet Gönen, Suleiman Khan, and Samuel Kaski. Kernelized bayesian matrix factorization. In *International Conference on Machine Learning*, pages 864–872, 2013.
- [21] Maxim Grechkin, Maryam Fazel, Daniela Witten, and Su-In Lee. Pathway graphical lasso. In *Twenty-Ninth AAAI Conference on Artificial Intelligence*, 2015.
- [22] Sogol Haghani and Mohammad Reza Keyvanpour. A systemic analysis of link prediction in social network. *Artificial Intelligence Review*, pages 1–35, 2017.
- [23] F Maxwell Harper and Joseph A Konstan. The movielens datasets: History and context. *Transactions on Interactive Intelligent Systems*, 5(4), 2015.
- [24] Jason Hartford, Devon R Graham, Kevin Leyton-Brown, and Siamak Ravanbakhsh. Deep models of interactions across sets. *arXiv preprint arXiv:1803.02879*, 2018.
- [25] T. Hastie, R. Tibshirani, and J. Friedman. *The Elements of Statistical Learning: Data Mining, Inference, and Prediction, Second Edition*. Springer Series in Statistics. Springer New York, 2009.

- [26] Edgar Jacoby and JB Brown. The future of computational chemogenomics. In *Computational Chemogenomics*, pages 425–450. Springer, 2018.
- [27] Alfredo Kalaitzis, John Lafferty, Neil Lawrence, and Shuheng Zhou. The bigraphical lasso. In *International Conference on Machine Learning*, pages 1229–1237, 2013.
- [28] Yehuda Koren, Robert Bell, and Chris Volinsky. Matrix factorization techniques for recommender systems. *Computer*, 2009.
- [29] S.L. Lauritzen. *Graphical Models*. Oxford science publications. Clarendon Press, 1996.
- [30] Kang Li, Jing Gao, Suxin Guo, Nan Du, Xiaoyi Li, and Aidong Zhang. Lrbm: A restricted boltzmann machine based approach for representation learning on linked data. In *2014 IEEE International Conference on Data Mining*, pages 300–309. IEEE, 2014.
- [31] Fei Liu, Sounak Chakraborty, Fan Li, Yan Liu, Aurelie C Lozano, et al. Bayesian regularization via graph laplacian. *Bayesian Analysis*, 9(2):449–474, 2014.
- [32] Yike Liu, Tara Safavi, Abhilash Dighe, and Danai Koutra. Graph summarization methods and applications: A survey. *ACM Computing Surveys (CSUR)*, 51(3):62, 2018.
- [33] Hao Ma, Dengyong Zhou, Chao Liu, Michael R Lyu, and Irwin King. Recommender systems with social regularization. In *Proceedings of the fourth ACM international conference on Web search and data mining*, pages 287–296. ACM, 2011.
- [34] Rahul Mazumder and Trevor Hastie. The graphical lasso: New insights and alternatives. *Electronic journal of statistics*, 6:2125, 2012.
- [35] Miller McPherson, Lynn Smith-Lovin, and James M Cook. Birds of a feather: Homophily in social networks. *Annual review of sociology*, 27(1):415–444, 2001.
- [36] Rachana Mehta and Keyur Rana. A review on matrix factorization techniques in recommender systems. In *2017 2nd International Conference on Communication Systems, Computing and IT Applications (CSCITA)*, pages 269–274. IEEE, 2017.
- [37] Andriy Mnih and Ruslan R Salakhutdinov. Probabilistic matrix factorization. In *Advances in neural information processing systems*, pages 1257–1264, 2008.
- [38] Federico Monti, Michael Bronstein, and Xavier Bresson. Geometric matrix completion with recurrent multi-graph neural networks. In *Advances in Neural Information Processing Systems*, pages 3697–3707, 2017.

- [39] Canh Hao Nguyen and Hiroshi Mamitsuka. Latent feature kernels for link prediction on sparse graphs. *IEEE transactions on neural networks and learning systems*, 23(11):1793–1804, 2012.
- [40] Nikhil Rao, Hsiang-Fu Yu, Pradeep K Ravikumar, and Inderjit S Dhillon. Collaborative filtering with graph information: Consistency and scalable methods. In *Advances in neural information processing systems*, pages 2107–2115, 2015.
- [41] H. Rue and L. Held. *Gaussian Markov Random Fields: Theory and Applications*. CRC Press, 2005.
- [42] Christos Sardinios, Grigorios Ballas Papadatos, and Iraklis Varlamis. Optimizing parallel collaborative filtering approaches for improving recommendation systems performance. *Information*, 10(5):155, 2019.
- [43] Kathrin Schacke. On the kronecker product. *Master’s thesis, University of Waterloo*, 2004.
- [44] Parag Singla and Matthew Richardson. Yes, there is a correlation:-from social networks to personal behavior on the web. In *Proceedings of the 17th international conference on World Wide Web*, pages 655–664. ACM, 2008.
- [45] Somayeh Sojoudi. Equivalence of graphical lasso and thresholding for sparse graphs. *The Journal of Machine Learning Research*, 17(1):3943–3963, 2016.
- [46] Somayeh Sojoudi. Graphical lasso and thresholding: Conditions for equivalence. In *Decision and Control (CDC)*, pages 7042–7048. IEEE, 2016.
- [47] Genevieve L Stein-O’Brien, Raman Arora, Aedin C Culhane, Alexander V Favorov, Lana X Garmire, Casey S Greene, Loyal A Goff, Yifeng Li, Aloune Ngom, Michael F Ochs, et al. Enter the matrix: factorization uncovers knowledge from omics. *Trends in Genetics*, 2018.
- [48] Jiliang Tang, Huiji Gao, and Huan Liu. mtrust: discerning multi-faceted trust in a connected world. In *Proceedings of the fifth ACM international conference on Web search and data mining*, pages 93–102. ACM, 2012.
- [49] Yangyang Xu and Wotao Yin. A block coordinate descent method for regularized multiconvex optimization with applications to nonnegative tensor factorization and completion. *SIAM Journal on imaging sciences*, 6(3):1758–1789, 2013.
- [50] Hongyang Xue, Shengming Zhang, and Deng Cai. Depth image inpainting: Improving low rank matrix completion with low gradient regularization. *IEEE Transactions on Image Processing*, 26(9):4311–4320, 2017.
- [51] Kai-Lang Yao and Wu-Jun Li. Convolutional geometric matrix completion. *arXiv preprint arXiv:1803.00754*, 2018.



- [52] Pooya Zakeri, Jaak Simm, Adam Arany, Sarah ElShal, and Yves Moreau. Gene prioritization using bayesian matrix factorization with genomic and phenotypic side information. *Bioinformatics*, 34(13):i447–i456, 2018.
- [53] Richard Zhang, Salar Fattahi, and Somayeh Sojoudi. Large-scale sparse inverse covariance estimation via thresholding and max-det matrix completion. In *Proceedings of the 35th International Conference on Machine Learning*, pages 5766–5775. PMLR, 2018.
- [54] He Zhao, Lan Du, and Wray Buntine. Leveraging node attributes for incomplete relational data. In *Proceedings of the 34th International Conference on Machine Learning-Volume 70*, pages 4072–4081. JMLR. org, 2017.
- [55] Z. Zhao, L. Zhang, X. He, and W. Ng. Expert finding for question answering via graph regularized matrix completion. *IEEE Transactions on Knowledge and Data Engineering*, 27(4):993–1004, April 2015.
- [56] Xiaodong Zheng, Hao Ding, Hiroshi Mamitsuka, and Shanfeng Zhu. Collaborative matrix factorization with multiple similarities for predicting drug-target interactions. In *Proceedings of the 19th ACM SIGKDD international conference on Knowledge discovery and data mining*, pages 1025–1033. ACM, 2013.
- [57] Tinghui Zhou, Hanhuai Shan, Arindam Banerjee, and Guillermo Sapiro. Kernelized probabilistic matrix factorization: Exploiting graphs and side information. In *Proceedings of the 2012 SIAM International Conference on Data Mining*, pages 403–414. SIAM, 2012.

## 6 Appendix

### A Posterior of GPMF model

We derive the posterior of  $\mathbf{U}$ , fixing  $\mathbf{V}$ , given the data  $\{\mathbf{R}, \mathbf{\Omega}\}$  and parameters  $\mathbf{\Lambda}_U$  for the Graph-based prior probabilistic matrix factoriation (GPMF) model. The posterior for  $\mathbf{V}$  follows the same steps with  $\mathbf{U}$  fixed. We start by breaking down the likelihood and prior into scalar operations:

$$\log p(\mathbf{R} | \mathbf{U}, \mathbf{V}, \alpha, \mathbf{\Lambda}_U) \quad (11)$$

$$\propto - \sum_{i=1}^N \sum_{j=1}^M \Omega_{ij} \left[ \frac{\alpha}{2} \left( \mathbf{R}_{ij} - \mathbf{U}_i \cdot \mathbf{V}_{j:}^\top \right)^2 \right] - \sum_{d=1}^D \frac{1}{2} \mathbf{U}_{:d}^\top \mathbf{\Lambda}_U \mathbf{U}_{:d} \quad (12)$$

$$= - \frac{\alpha}{2} \sum_{i=1}^N \sum_{j=1}^M \Omega_{ij} \left[ \left( \mathbf{R}_{ij}^2 - 2\mathbf{R}_{ij} \sum_{d=1}^D \mathbf{U}_{id} \mathbf{V}_{jd} + \sum_{d=1}^D \sum_{d'=1}^D \mathbf{V}_{jd} \mathbf{U}_{id} \mathbf{U}_{id'} \mathbf{V}_{jd'} \right) \right] \quad (13)$$

$$- \frac{1}{2} \sum_{d=1}^D \sum_{i=1}^N \sum_{i'=1}^N \mathbf{U}_{id} [\mathbf{\Lambda}_U]_{ii'} \mathbf{U}_{i'd} \quad (14)$$

$$= - \frac{\alpha}{2} \sum_{i=1}^N \sum_{j=1}^M \Omega_{ij} \mathbf{R}_{ij}^2 - \frac{1}{2} \sum_{i=1}^N \left( \alpha \sum_{j=1}^M \Omega_{ij} \sum_{d=1}^D \sum_{d'=1}^D [\mathbf{V}_{jd} \mathbf{U}_{id} \mathbf{U}_{id'} \mathbf{V}_{jd'} \right. \quad (15)$$

$$\left. - 2\mathbf{U}_{id} \mathbf{V}_{jd} \mathbf{R}_{ij} \right] + \sum_{d=1}^D \sum_{i'=1}^N \mathbf{U}_{id} [\mathbf{\Lambda}_U]_{ii'} \mathbf{U}_{i'd} \Big). \quad (16)$$

$$(17)$$

Using the scalar expansion we recombine to form the full posterior in scalar form in Equation (21), with respect to the vectorization of  $\mathbf{U}$  Equation (23) and w.r.t.

the vectorization of  $\mathbf{U}^\top$  Equation (24):

$$\begin{aligned}
& \log p(\mathbf{U} \mid \mathbf{R}, \alpha, \mathbf{V}, \mathbf{\Lambda}_U) \tag{18} \\
& \propto -\frac{1}{2} \sum_{i=1}^N \sum_{j=1}^M \sum_{d=1}^D \left( \alpha \mathbf{\Omega}_{ij} \left[ \sum_{d'=1}^D \mathbf{V}_{jd} \mathbf{U}_{id} \mathbf{U}_{id'} \mathbf{V}_{jd'} - 2 \mathbf{U}_{id} \mathbf{V}_{jd} \mathbf{R}_{ij} \right] + \sum_{i'=1}^N \mathbf{U}_{id} [\mathbf{\Lambda}_U]_{ii'} \mathbf{U}_{i'd} \right) \tag{19} \\
& = -\frac{1}{2} \sum_{i=1}^N \sum_{d=1}^D \mathbf{U}_{id} \left( \alpha \sum_{j=1}^M \mathbf{\Omega}_{ij} \left[ \sum_{d'=1}^D \mathbf{V}_{jd} \mathbf{U}_{id'} \mathbf{V}_{jd'} - 2 \mathbf{V}_{jd} \mathbf{R}_{ij} \right] + \sum_{i'=1}^N [\mathbf{\Lambda}_U]_{ii'} \mathbf{U}_{i'd} \right) \tag{20} \\
& = -\frac{1}{2} \sum_{i=1}^N \sum_{i'=1}^N \sum_{d=1}^D \sum_{d'=1}^D \left[ \mathbf{U}_{id} \left( \alpha \sum_{j=1}^M [i=i'] I_{ij} \mathbf{V}_{jd} \mathbf{V}_{jd'} + [d=d'] [\mathbf{\Lambda}_U]_{ii'} \right) \mathbf{U}_{i'd} \right. \tag{21} \\
& \quad \left. - 2 \alpha \mathbf{U}_{id} \mathbf{V}_{jd} \mathbf{R}_{ij} \right] \tag{22} \\
& = -\frac{1}{2} \text{vec}(\mathbf{U})^\top (I_D \otimes \mathbf{\Lambda}_U + \alpha \mathbf{C}) \text{vec}(\mathbf{U}) - 2 \alpha \text{Tr}(\mathbf{U}^\top \mathbf{R} \mathbf{V}) \tag{23} \\
& = -\frac{1}{2} \text{vec}(\mathbf{U}^\top)^\top \left( \mathbf{\Lambda}_U \otimes I_D + \alpha \text{blkdiag} \left( \{\mathbf{B}_i\}_{i=1}^N \right) \right) \text{vec}(\mathbf{U}^\top) - 2 \alpha \text{Tr}(\mathbf{U} \mathbf{V}^\top \mathbf{R}^\top), \tag{24}
\end{aligned}$$

where  $[i=j]$  is Iverson bracket notation where the value is one if the proposition is satisfied and zero otherwise,  $\otimes$  is the Kronecker product,  $\text{vec}(\mathbf{X})$  stacks the columns of matrix  $\mathbf{X}$  to produce a vector,  $\text{Tr}(\mathbf{X})$  is the trace of matrix  $\mathbf{X}$  and finally  $I_N$  is an  $N \times N$  identity matrix and:

$$\mathbf{C} = \begin{bmatrix} \mathbf{c}(1,1) & \mathbf{c}(1,2) & \cdots & \mathbf{c}(1,D) \\ \mathbf{c}(2,1) & \mathbf{c}(2,2) & \cdots & \mathbf{c}(2,D) \\ \vdots & \vdots & \ddots & \vdots \\ \mathbf{c}(D,1) & \mathbf{c}(D,2) & \cdots & \mathbf{c}(D,D) \end{bmatrix} \tag{25}$$

$$\mathbf{c}(d, d') = \text{diag} \left( \left\{ \sum_{j=1}^M \mathbf{\Omega}_{ij} \mathbf{V}_{jd} \mathbf{V}_{jd'} \right\}_{i=1}^N \right) \tag{26}$$

$$\mathbf{B}_i = \sum_{\{j:(i,j) \in \{\mathbf{\Omega}=1\}\}} \mathbf{V}_j^\top \mathbf{V}_j \tag{27}$$

Notice that in the posterior when stacking the columns  $\text{vec}(\mathbf{U})$  in Equation (23) the prior precision matrix is a block diagonal matrix and the evidence matrix is a partitioned matrix with each block being diagonal, when stacking the rows  $\text{vec}(\mathbf{U}^\top)$  the structural pattern is the other way around: the prior is a partitioned matrix of diagonal blocks and the evidence matrix is a block diagonal matrix. It is worth noting that Equation (23) and Equation (24) both have the structure of a Kronecker sum,  $\mathbf{A} \oplus \mathbf{D} = \mathbf{A} \otimes I + I \otimes \mathbf{D}$ . We look more closely at Equation (24),

showing the relation with the scalar summations and the final notation in more detail. Firstly the linear term:

$$-2\alpha \sum_{i=1}^N \sum_{d=1}^D \mathbf{U}_{id} \sum_{j=1}^M \Omega_{ij} \mathbf{V}_{jd} \mathbf{R}_{ij} = -2\alpha \sum_{i=1}^N \sum_{d=1}^D \mathbf{U}_{id} \sum_{j=1}^M \mathbf{V}_{jd} \mathbf{R}_{ij} \quad (28)$$

$$= -2\alpha \sum_{d=1}^D \mathbf{U}_{:d}^\top \mathbf{R} \mathbf{V}_{:d} \quad (29)$$

$$= -2\alpha \text{vec}(\mathbf{U})^\top \text{vec}(\mathbf{R} \mathbf{V}) \quad (30)$$

$$= -2\alpha \text{Tr}(\mathbf{U}^\top \mathbf{R} \mathbf{V}) \quad (31)$$

$$= -2\alpha \sum_{i=1}^N \mathbf{U}_i \mathbf{V}^\top [\mathbf{R}_{i:}]^\top \quad (32)$$

$$= -2\alpha \text{vec}(\mathbf{U}^\top)^\top \text{vec}(\mathbf{V}^\top \mathbf{R}^\top) \quad (33)$$

$$= -2\alpha \text{Tr}(\mathbf{U} \mathbf{V}^\top \mathbf{R}^\top) \quad , \quad (34)$$

and the quadratic term:

$$\sum_{i=1}^N \sum_{i'=1}^N \sum_{d=1}^D \sum_{d'=1}^D \mathbf{U}_{id} \sum_{j=1}^M [i=i'] [\mathbf{V}_{jd} \mathbf{V}_{jd'}] \mathbf{U}_{i'd'} = \text{vec}(\mathbf{U})^\top \left[ \sum_{j=1}^M \mathbf{V}_j^\top \mathbf{V}_j \otimes I_N \right] \text{vec}(\mathbf{U}) \quad (35)$$

$$= \text{vec}(\mathbf{U})^\top \left[ \text{diag} \left\{ \sum_{j=1}^M \mathbf{V}_j^\top \mathbf{V}_j \right\} \right]_N \text{vec}(\mathbf{U}) \quad (36)$$

$$\sum_{i=1}^N \sum_{i'=1}^N \sum_{d=1}^D \sum_{d'=1}^D \mathbf{U}_{id} [d=d'] [\mathbf{\Lambda}_U]_{ii'} \mathbf{U}_{i'd'} = \text{vec}(\mathbf{U})^\top [\mathbf{\Lambda}_U \otimes I_D] \text{vec}(\mathbf{U}) \quad (37)$$

$$= \text{vec}(\mathbf{U}^\top)^\top [I_D \otimes \mathbf{\Lambda}_U] \text{vec}(\mathbf{U}^\top) \quad (38)$$

Having organized the posterior, with respect to  $\mathbf{U}$ , into a quadratic and a linear term we can complete the square to find the mean  $\boldsymbol{\mu}_U^{(n)}$  and precision matrix  $\boldsymbol{\Lambda}_U^{(n)}$  of the conditional posterior distribution for the matrix  $\mathbf{U}$ :

$$\boldsymbol{\Lambda}_U^{(n)} = [\mathbf{\Lambda}_U \otimes I_D] + \alpha \text{blkdiag} \left( \{\mathbf{B}_i\}_{i=1}^N \right) \quad (39)$$

$$\boldsymbol{\mu}_U^{(n)} = \left[ \boldsymbol{\Lambda}_U^{(n)} \right]^{-1} \text{vec}(\mathbf{V}^\top \mathbf{R}^\top) \quad (40)$$

or the mean and covariance can be represented as different formulations with scalar sums (22), or vectorization of the matrix without transposing (23).

## B Experiments: further details

All experiments were run on a regular laptop computer: Hewlett Packard EliteBook 840 G3 notebook with Intel Core i5 and 16 GiB memory.

We compare our GPMF method to GRALS<sup>2</sup> [40], PMF (GRALS with no graph side-information) [37] and KPMF<sup>3</sup> [57]. KPMF uses the regularised Laplacian graph kernel. KBMF also uses the regularised Laplacian graph kernel. We allow the algorithms to have approximately the same running time, for fair comparison. It’s worth noting that KBMF has many tuning parameters and a slow learning speed, making parameter tuning costly and complex, with similar effort as made for tuning the other algorithms we were not able to attain good results with KBMF. We ran the geometric deep learning model<sup>4</sup> [38] but on MovieLens 100k, which took the other models a few minutes to converge, it ran for over two hours without converging, see Figure 8 (left). Therefore we concluded that this model requires parallel GPUs to be scalable and is not comparable to the computationally efficient methods we are interested in. For model learning and evaluation we use a training and validation set. We explore a small number of tuning parameter options and put use the same search procedure (similar effort for tuning) for each model for a fair comparison. We also show the advantage of the updated graph below by running KPMF and geometric deep learning [38] comparing the original and updated graph.

### B.1 Synthetic Data

Default settings for the experiments, if no other details are mentioned, are a  $400 \times 400$  data matrix with 7 percent observed values, a graph fidelity of 0.7, observation noise  $\sigma^2 = 0.01$ , 40 latent feature dimensions and noise between similar latent features 0.0001. We use the graphs to create the latent feature matrices  $\mathbf{U}$  and  $\mathbf{V}$  according to the GPMF model. Sampling of observed entries for training and validation is according to a non-uniform distribution; to avoid rows and columns having similar numbers of observations, we use a multinomial distribution with Dirichlet prior). Each experiment setting is run five times for each model and an average is reported with the standard deviation as the height of the error bar.

### B.2 Real data experiments

**Flixster (3k).** A three thousand dimensional subset matrix from the original Flixster dataset<sup>5</sup> as in [38]. Where graph side information is constructed from the scores of the original matrix:  $\mathbf{G}_U$  with 59354 edges and  $\mathbf{G}_V$  50918 edges.

<sup>2</sup>GRALS code: <https://github.com/rofuyu/exp-grmf-nips15>

<sup>3</sup>KPMF code: <https://people.eecs.berkeley.edu/tinghuiz/>

<sup>4</sup>Recurrent Multi-Graph Neural Networks code: <https://github.com/fmonti/mgcn>

<sup>5</sup><https://github.com/fmonti/mgcn>

**Douban (3k).** A three thousand dimensional subset matrix from the original Douban dataset<sup>6</sup> as in [38]. Where user graph side-information is a social network with 2688 edges.

**MovieLens 100k and 20M.** The GroupLens official MovieLens<sup>7</sup> 100k and 20M datasets [23]. For MovieLens 100k graph side-information is constructed for users, based on user demographic information using k-nearest neighbour (kNN) algorithm with ten neighbours. For MoveLens 20M graph side-information is constructed using kNN with  $k=\{10,20,40\}$  based on movie genre data with 492956, 962644 and 1870508 edges respectively.

**Epinions.** We take the Epinions<sup>8</sup> dataset as described in KPMF, but we use a much larger data size<sup>9</sup> (22164 x 296277) with user trust network data (22164 x 22164) [48]. The dataset is extremely sparse (9.8312e-05 proportion of observed entries), and distributed un-uniformly, making this a difficult problem.

**YahooMusic** The official Yahoo Music ratings data from the KDD cup [15] as used in [40] to demonstrate scalability. We construct the graph with exact kNN on the music covariate data (artist,genre,album) with ten neighbours. This results in a very sparse graph, likely connecting many music tracks from the same artist and in the same album only.

**Model tuning** Data is split into test and validation. We use a procedure of parameter searching that we repeat for each model. PMF observation noise is fixed at  $\sigma^2 = 1$ . PMF, GRALS and GPMF use the same CG iterations configuration (CG). GPMF uses  $\tau = 0$  for thresholding. KPMF uses the regularised Laplacian graph kernel with graph strength  $\gamma$  and learning rate  $\epsilon$ . KBMF is trained with uninformative priors:  $(\alpha_\lambda = 1, \beta_\lambda = 1)$ , changing these values we saw no improvements; with at most one graph for each kernel multi-kernel parameters do not require tuning.

**General use of updated graph** We believe that removing the *contested* edges improves the graph for this task in general for any model, not just for GPMF. To this end we tested this by using the full graph vs. updated graph for KPMF [57] and for a completely different model, Geometric deep learning [38]. The results, in Figure 8, were improved speed and accuracy for KPMF. For the deep learning model, we ran it for several hours without convergence with the provided code (on a standard laptop) and did not wait until convergence, but we did see that the model seemed to be converging faster with the updated graph.

---

<sup>6</sup>See footnote 1

<sup>7</sup><https://grouplens.org/datasets/movielens/>

<sup>8</sup>[www.epinions.com](http://www.epinions.com)

<sup>9</sup><https://www.cse.msu.edu/~tangjili/trust.html> , <https://www.cse.msu.edu/~tangjili/datasetcode/epinions.zip>

Table 2: Model parameter tuning for real world experiments

	FLIXSTER (3K)	DOUBAN (3K)	MOVIELENS 100K	EPINIONS
D=	10	10	10	10
PMF ( $\sigma_U, \sigma_V, CG$ )	0.1,0.1,1	5,5,1	1.2,1.2,2	0.75,0.2,3
GRALS ( $\lambda_L, \lambda_U, \lambda_V$ )	3,0.5,0.5	8,2,5	0.1,0.01,0.01	0.01,0.01,0.02
GPMF ( $\sigma_2, \lambda_L, \lambda_U, \lambda_V$ )	1,5,1,1	0.5,5,2,5	0.05,1,0.05,0.05	0.1,0.1,0.1,0.1
KPMF ( $\sigma^2, \epsilon, \gamma_U, \gamma_V$ )	0.1, $10^{-6}$ , 1, 1	0.07, $10^{-6}$ , 100, 100	0.2, $10^{-5}$ , 1.1, 1.1	N/A
KBMF ( $\gamma_U, \gamma_V, \sigma_g, \sigma_y$ )	1,1,0.1,1	1,1,0.2,1	0.35,0.3,0.1,0.15	N/A
	YAHOO MUSIC	MOVIELENS 20M 10NN	20NN	40NN
D=	20	10	10	10
PMF ( $\sigma_U, \sigma_V, CG$ )	10,10	1.25,12.5,10	1.25,12.5,10	1.25,12.5,10
GRALS ( $\lambda_L, \lambda_U, \lambda_V$ )	100,200	5,0.5,0.01	1,1,10	1,1,10
GPMF ( $\sigma_2, \lambda_L, \lambda_U, \lambda_V$ )	10,10,100,200	0.05,5,0.1,0.01	0.5,5,0.1,0.1	0.5,2.5,0.01,0.01

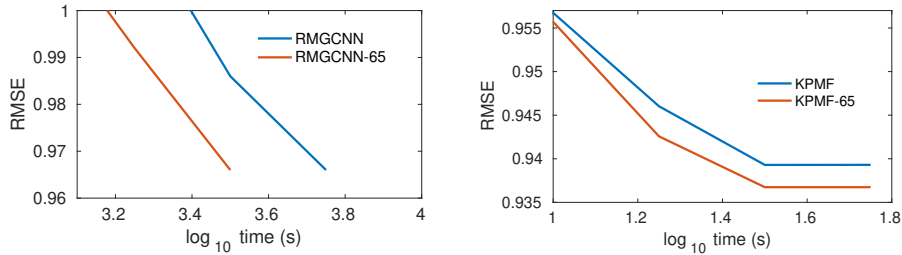


Figure 8: Convergence time on MovieLens 100k. We provide an updated graph with 65% of the edges learnt with GPMF to the state-of-the-art recurrent multi-graph neural network [38] (left) and to another graph-regularised matrix factorisation method (KPMF [57], right) to show that the optimised graph improves the convergence (left and right) and precision (right) of arbitrary algorithms for the graph regularised matrix completion problem.